EMBRY-RIDDLE
Aeronautical University
SCHOLARLY COMMONS

Publications

11-2019

An Explicit Finite Volume Numerical Scheme for 2D Elastic Wave Propagation

Mihhail Berezovski
Embry-Riddle Aeronautical University, berezovm@erau.edu

Arkadi Berezovski
Tallinn University of Technology, arkadi.berezovski@cs.ioc.ee

Follow this and additional works at: https://commons.erau.edu/publication

 Part of the Other Mathematics Commons

Scholarly Commons Citation

Berezovski, M., & Berezovski, A. (2019). An Explicit Finite Volume Numerical Scheme for 2D Elastic Wave Propagation. *Applied Wave Mathematics II, 6*(). https://doi.org/10.1007/978-3-030-29951-4_12

This Book Chapter is brought to you for free and open access by Scholarly Commons. It has been accepted for inclusion in Publications by an authorized administrator of Scholarly Commons. For more information, please contact commons@erau.edu.

An explicit finite volume numerical scheme for 2D elastic wave propagation

Mihhail Berezovski and Arkadi Berezovski

Abstract The construction of the two-dimensional finite volume numerical scheme based on the representation of computational cells as thermodynamic systems is presented explicitly. The main advantage of the scheme is an accurate implementation of conditions at interfaces and boundaries. It is demonstrated that boundary conditions influence the wave motion even in the simple case of a homogeneous waveguide.

1 Introduction

Problems in wave propagation in elastic solids can be formulated in terms of hyperbolic conservation laws. Due to the great importance of conservation laws (Dafermos, 2010), a lot of numerical methods were applied to their solution: finite difference methods (Godlewski and Raviart, 1996; Trangenstein, 2009), finite element methods (Cohen, 2002; Kampanis et al., 2008), discontinuous Galerkin methods (Hesthaven and Warburton, 2007; Cohen and Pernet, 2017), finite volume methods (LeVeque, 2002; Guinot, 2003), spectral methods (Hesthaven et al., 2007; Gopalakrishnan et al., 2007) etc. The comprehensive survey of numerical methods for conservation laws is presented recently (Hesthaven, 2018). Nevertheless, there still exist problems with interface and boundary conditions in multi-dimensional cases (Gao et al., 2015). In this paper we are focusing on the construction of a two-dimensional explicit finite volume numerical scheme with the special attention to the implementation of boundary conditions.

Mihhail Berezovski
Embry–Riddle Aeronautical University, Daytona Beach, FL e-mail: mihhail.berezovski@erau.edu

Arkadi Berezovski
Tallinn University of Technology, School of Science, Tallinn, Estonia e-mail: arkadi.berezovski@cs.ioc.ee

1.1 Finite volume methods

Finite volume schemes are powerful numerical methods for solving nonlinear conservation laws and related equations. Such methods are locally conservative and based on cell averages. The numerical solution of systems of hyperbolic conservation laws is dominated by Riemann-solver-based schemes (Godlewski and Raviart, 1996; Toro, 1997; LeVeque, 2002; Guinot, 2003). The upgrade of the solution in a given cell is determined by the exchanges (via fluxes) at the interfaces with the neighbouring cells. The fluxes are computed by solving Riemann problems at the interfaces between neighboring cells.

Computing an exact solution to the Riemann problem can be a very time-consuming task because an iterative procedure is needed. Therefore, approximate Riemann solvers are often preferred because they provide satisfactory solutions while using faster algorithms. Two broad families of solvers can be distinguished: (i) solvers where the Riemann problem is simplified (e.g. by linearizing the equations), and (ii) solvers where simplified relationships are used to solve the exact problem. The first family of solver includes Roe's solver (Roe, 1981), where the flux at the location of the initial discontinuity is calculated via a wave decomposition under the assumption of a constant Jacobian matrix. The Jacobian matrix is approximated in such a way that consistency and conservation conditions are satisfied. An entropy fix is needed when a rarefaction wave extends over the location of the initial discontinuity. From another side, primitive variable Riemann solvers (Toro, 1997) use a linearization of the hyperbolic system with a constant Jacobian matrix in combination with the Rankine–Hugoniot conditions across each wave. This allows a simplified system of equations to be solved for the unknown variables. The Riemann invariants can also be used along the characteristics to obtain the simplified system (Lhomme and Guinot, 2007).

1.2 Higher-order accuracy

However, the cell average of a solution in a cell contains too little information. In order to obtain higher-order accuracy, neighboring cell averages are used to reconstruct an approximate polynomial solution in each cell. This reconstruction procedure is the key step for many high-resolution schemes (Liu et al., 2007). For example, in the ADER approach (Titarev and Toro, 2002), the numerical flux function is based on the solution of generalized Riemann problems, where the initial data on both sides of the element interfaces are no longer piecewise constant. Here the initial data is piecewise polynomial, in general separated by a jump at the interface. The fundamental idea behind the generalized Riemann problem solvers is a temporal Taylor series expansion of the state at the interface, where then time derivatives are replaced by space derivatives using repeatedly the governing conservation law in differential form, which is the so-called Cauchy–Kovalewski or Lax–Wendroff procedure (Dumbser and Käser, 2007).

1.3 Higher dimensions

When extending the flux-difference schemes to multi-dimensional problems, the so-called grid aligned finite volume approach or dimensional splitting method is adopted traditionally using one-dimensional Riemann solvers. However, for multi-dimensional problem, there is in general no longer a finite number of directions of information propagation. It has been pointed out (Roe, 1986) that the Riemann-solver is applied in the grid- rather than the flow-direction, which may lead to a misinterpretation of the local wave structure of the solution. To overcome the drawbacks of methods based on dimensional splitting, there have been considerable efforts to develop so-called genuinely multi-dimensional schemes for solving hyperbolic conservation laws (Colella, 1990; Billett and Toro, 1997; LeVeque, 2002; Guinot, 2003).

1.4 Discontinuities

While the abovementioned numerical methods have been successfully applied to the solution of problems with smoothly varying fields, they cannot readily handle evolving discontinuities like cracks or martensitic phase-transition fronts inside bodies (de Borst, 2008). The reason is the absence of the constitutive information to specify the velocity of the discontinuity uniquely (Abeyaratne and Knowles, 2006). In the series of papers (Berezovski and Maugin, 2004, 2005a, 2007; Maugin and Berezovski, 2009; Berezovski and Maugin, 2010), it is shown how the additional constitutive information can be extracted from the analysis of the non-equilibrium interaction between two discrete thermodynamic systems. Moreover, this additional information has been successfully embedded into a finite volume algorithm for thermoelastic wave and front propagation represented in terms of averaged and excess quantities (Berezovski et al., 2000; Berezovski and Maugin, 2001, 2002; Berezovski et al., 2003; Berezovski and Maugin, 2005b; Berezovski et al., 2006, 2008; Berezovski, 2011). It should be noted that in the one-dimensional case this algorithm can be identified with the conservative wave-propagation algorithm (Bale et al., 2003) for smooth solutions (Berezovski, 2011). This means that the splitting of one-dimensional fluxes in the transverse directions in the spirit of the wave-propagation algorithm (LeVeque, 1997) is still possible, but only for smooth solutions.

1.5 The structure of the paper

To obtain the multi-dimensional description of evolving discontinuities we need to extend the algorithm in terms of averaged an excess quantities onto at least two dimensions. This is the main aim of the paper, which is devoted to the derivation and the application of the two-dimensional finite volume numerical scheme for elastic

wave propagation. The paper is organized as follows. In Section 2 the governing equations of linear elasticity are presented in the plane strain approximation. Then the finite volume numerical scheme is deduced in Section 3 on the regular cartesian grid. The algebraic relations for excess quantities are written down explicitly in Section 4. Boundary conditions are formulated on the example of the test problem of wave propagation in an homogeneous waveguide. Results of calculations of the test problem are presented in Section 5. Conclusions are given in the last Section.

2 Governing equations

Elastic solids are characterized by the Hooke law which can be represented in the isotropic case in the form of the stress-strain relation (Mase et al., 2009)

$$\sigma_{ij} = \lambda \delta_{ij} \varepsilon_{kk} + 2\mu \varepsilon_{ij}, \tag{1}$$

with the Cauchy stress tensor σ_{ij}, the strain tensor ε_{ij}, and the Lamé parameters λ and μ. In the linear elasticity, a motion is governed by the local balance of linear momentum at each regular material point (Achenbach, 1973)

$$\rho \frac{\partial v_i}{\partial t} = \frac{\partial \sigma_{ij}}{\partial x_i} + f_i, \tag{2}$$

where ρ is the matter density, v_i is the particle velocity, t is time, f_i is a body force, and x_i are spatial coordinates.

We consider the plane strain situation which means that a body is extremely thick along one coordinate, say, z, and where all applied forces are uniform in the z direction. Since all derivatives with respect to z vanish, all fields can be viewed as functions of x and y alone. In the plane strain case in the absence of body force, the governing equations for wave motion (2) are reduced to

$$\rho \frac{\partial v_1}{\partial t} = \frac{\partial \sigma_{11}}{\partial x} + \frac{\partial \sigma_{12}}{\partial y}, \tag{3}$$

$$\rho \frac{\partial v_2}{\partial t} = \frac{\partial \sigma_{21}}{\partial x} + \frac{\partial \sigma_{22}}{\partial y}. \tag{4}$$

Stress-strain relations (1) are reformulated accordingly

$$\sigma_{11} = (\lambda + 2\mu)\varepsilon_{11} + \lambda \varepsilon_{22}, \tag{5}$$

$$\sigma_{12} = \sigma_{21} = 2\mu \varepsilon_{12}, \tag{6}$$

$$\sigma_{22} = (\lambda + 2\mu)\varepsilon_{22} + \lambda \varepsilon_{11}. \tag{7}$$

Time derivatives of stress-strain relations (5) – (7) can be represented in terms of velocities

$$\frac{\partial \sigma_{11}}{\partial t} = (\lambda + 2\mu)\frac{\partial v_1}{\partial x} + \lambda \frac{\partial v_2}{\partial y}, \tag{8}$$

$$\frac{\partial \sigma_{22}}{\partial t} = \lambda \frac{\partial v_1}{\partial x} + (\lambda + 2\mu)\frac{\partial v_2}{\partial y}, \tag{9}$$

$$\frac{\partial \sigma_{12}}{\partial t} = \frac{\partial \sigma_{21}}{\partial t} = \mu \left(\frac{\partial v_1}{\partial y} + \frac{\partial v_2}{\partial x} \right), \tag{10}$$

because strains and velocities are connected by compatibility conditions

$$\frac{\partial \varepsilon_{11}}{\partial t} = \frac{\partial v_1}{\partial x}, \tag{11}$$

$$\frac{\partial \varepsilon_{12}}{\partial t} = \frac{1}{2} \left(\frac{\partial v_1}{\partial y} + \frac{\partial v_2}{\partial x} \right), \tag{12}$$

$$\frac{\partial \varepsilon_{22}}{\partial t} = \frac{\partial v_2}{\partial y}. \tag{13}$$

Equations (8) – (10) together with the balance of linear momentum (3)–(4) form the closed system of equations, which is convenient for a numerical solution. In what follows it will be demonstrated how an explicit finite volume numerical scheme can be constructed which is suitable for the implementation of boundary and interface conditions in a natural way.

3 Discretization

3.1 Averaged and excess quantities

The first step in the construction of the numerical algorithm is the spatial discretisation of the computational domain. Let us introduce a Cartesian grid of cells $C_{nm} = [x_n, x_{n+1}] \times [y_m, y_{m+1}]$ with interfaces $x_n = n\Delta x, y_m = m\Delta y$, and time levels $t_k = k\Delta t$. For simplicity, the grid size $\Delta x, \Delta y$ and time step Δt are assumed to be constant. The values of wanted fields are somehow distributed across the cells.

The main idea in the construction of the algorithm is the consideration of every computational cell as a thermodynamic system (Muschik and Berezovski, 2004). Since we cannot expect that such thermodynamic system is in equilibrium, its local equilibrium state is described by averaged values of field quantities. The use of cell averages is the standard procedure in the finite-volume methods. What is non-standard that is the introduction into consideration so-called "excess quantities" in the spirit of the thermodynamics of discrete systems (Muschik and Berezovski, 2004).

The excess quantities represent the difference between values of true and averaged quantities (Berezovski et al., 2008):

$$v_i = \overline{v}_i + V_i, \quad \sigma_{ij} = \overline{\sigma}_{ij} + \Sigma_{ij}. \tag{14}$$

Here overbars denote averaged quantities and capital letters relate to excess quantities.

3.2 Integration over the cell

Keeping in mind the representation of field quantities mentioned above, we integrate the governing equations over the computational cell. The integration of the first component of the balance of linear momentum reads

$$\begin{aligned}
&\int_{\Delta x}\int_{\Delta y}\rho\dot{v}_1 dxdy = \int_{\Delta y}\left(\sigma^r_{11}-\sigma^l_{11}\right)dy+\int_{\Delta x}\left(\sigma^t_{12}-\sigma^b_{12}\right)dx\\
&=\int_{\Delta y}\left(\overline{\sigma}_{11}+\Sigma^r_{11}-\overline{\sigma}_{11}-\Sigma^l_{11}\right)dy+\int_{\Delta x}\left(\overline{\sigma}_{12}+\Sigma^t_{12}-\overline{\sigma}_{12}-\Sigma^b_{12}\right)dx= \qquad (15)\\
&=\int_{\Delta y}\left(\Sigma^r_{11}-\Sigma^l_{11}\right)dy+\int_{\Delta x}\left(\Sigma^t_{12}-\Sigma^b_{12}\right)dx,
\end{aligned}$$

where upper indices r,l,u,b denote "right side", "left side", "top", and "bottom", respectively (Fig. 1).

As one can see, the result of the integration is expressed in terms of excess quantities at the boundaries of the cell. These quantities, however, are not constants but vary along the corresponding boundary.

3.2.1 Parabolic approximation at cell boundaries

To proceed further, we need to approximate the unknown functions $\Sigma^r_{11}(y),\Sigma^l_{11}(y)$ and $\Sigma^t_{12}(x),\Sigma^b_{12}(x)$. Suppose that we know the values $\Sigma^{rt}_{11},\Sigma^{rb}_{11}$ at right-top and right-bottom corners and the value Σ^{rc}_{11} in the middle point for the right boundary of the cell numbered by "n,m". Then we can approximate the function $\Sigma^r_{11}(y)$ by a quadratic dependence. According to the Simpson rule, we can compute the first integral in $(15)_3$ as follows:

$$\int_{\Delta y}\Sigma^r_{11}dy=\Delta y\left(\frac{2}{3}\Sigma^{rc}_{11}+\frac{1}{6}\left(\Sigma^{rt}_{11}+\Sigma^{rb}_{11}\right)\right).$$

The similar procedure can be applied for the calculation of all integrals in $(15)_3$. Therefore, the integration of the first component of the balance of linear momentum results in the relationship for each computational cell

$$\begin{aligned}
\int_{\Delta x}\int_{\Delta y}\rho\dot{v}_1 dxdy \approx{}& \frac{2}{3}\Delta y\left(\Sigma^{rm}_{11}-\Sigma^{lm}_{11}\right)+\frac{1}{6}\Delta y\left(\Sigma^{rt}_{11}+\Sigma^{rb}_{11}-\Sigma^{lt}_{11}-\Sigma^{lb}_{11}\right)+\\
&+\frac{2}{3}\Delta x\left(\Sigma^{tc}_{12}-\Sigma^{bc}_{12}\right)+\frac{1}{6}\Delta x\left(\Sigma^{tr}_{12}+\Sigma^{tl}_{12}-\Sigma^{br}_{12}-\Sigma^{bl}_{12}\right),
\end{aligned} \qquad (16)$$

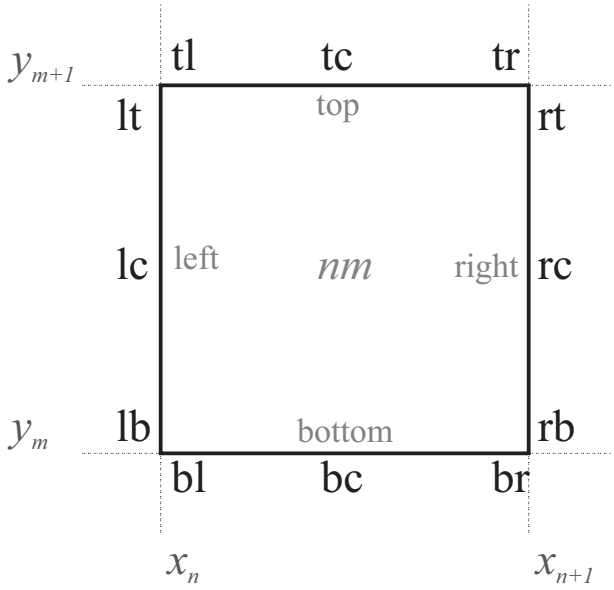

Fig. 1 Notation for a cell

where a combination of two upper indices means the value of the excess quantity at the corresponding corner or middle point (Fig. 1). Accordingly, for the second component of the balance of linear momentum we have

$$\begin{aligned}
&\int_{\Delta x}\int_{\Delta y}\rho\dot{v}_2 dxdy = \int_{\Delta y}\left(\sigma^r_{21}-\sigma^l_{21}\right)dy + \int_{\Delta x}\left(\sigma^t_{22}-\sigma^b_{22}\right)dx \\
&= \int_{\Delta y}\left(\overline{\sigma}_{21}+\Sigma^r_{21}-\overline{\sigma}_{21}-\Sigma^l_{21}\right)dy + \int_{\Delta x}\left(\overline{\sigma}_{22}+\Sigma^t_{22}-\overline{\sigma}_{22}-\Sigma^b_{22}\right)dx = \\
&= \int_{\Delta y}\left(\Sigma^r_{21}-\Sigma^l_{21}\right)dy + \int_{\Delta x}\left(\Sigma^t_{22}-\Sigma^b_{22}\right)dx \approx \\
&\approx \frac{2}{3}\Delta y\left(\Sigma^{rc}_{21}-\Sigma^{lc}_{21}\right)+\frac{1}{6}\Delta y\left(\Sigma^{rt}_{21}+\Sigma^{rb}_{21}-\Sigma^{lt}_{21}-\Sigma^{lb}_{21}\right)+ \\
&+ \frac{2}{3}\Delta x\left(\Sigma^{tc}_{22}-\Sigma^{bc}_{22}\right)+\frac{1}{6}\Delta x\left(\Sigma^{tr}_{22}+\Sigma^{tl}_{22}-\Sigma^{br}_{22}-\Sigma^{bl}_{22}\right).
\end{aligned} \tag{17}$$

Similarly, the integration of time derivatives of stress-strain relations (8)–(10) leads to

$$
\begin{aligned}
&\int_{\Delta x}\int_{\Delta y}\dot{\sigma}_{11}dxdy = (\lambda+2\mu)\int_{\Delta y}\left(v_1^r - v_1^l\right)dy + \lambda\int_{\Delta x}\left(v_2^t - v_2^b\right)dx = \\
&= (\lambda+2\mu)\int_{\Delta y}\left(\overline{v}_1 + V_1^r - \overline{v}_1 - V_1^l\right)dy + \lambda\int_{\Delta x}\left(\overline{v}_2 + V_2^t - \overline{v}_2 - V_2^b\right)dx = \\
&= (\lambda+2\mu)\int_{\Delta y}\left(V_1^r - V_1^l\right)dy + \lambda\int_{\Delta x}\left(V_2^t - V_2^b\right)dx \approx \\
&\approx \frac{2}{3}(\lambda+2\mu)\Delta y\left(V_1^{rc} - V_1^{lc}\right) + (\lambda+2\mu)\frac{1}{6}\Delta y\left(V_1^{rt} + V_1^{rb} - V_1^{lt} - V_1^{lb}\right) + \\
&+ \frac{2}{3}\lambda\Delta x\left(V_2^{tc} - V_2^{bc}\right) + \lambda\frac{1}{6}\Delta x\left(V_2^{tr} + V_2^{tl} - V_2^{br} - V_2^{bl}\right),
\end{aligned}
\tag{18}
$$

for the first normal component of the stress tensor,

$$
\begin{aligned}
&\int_{\Delta x}\int_{\Delta y}\dot{\sigma}_{12}dxdy = \frac{\mu}{2}\int_{\Delta y}\left(v_2^r - v_2^l\right)dy + \frac{\mu}{2}\int_{\Delta x}\left(v_1^t - v_1^b\right)dx = \\
&= \frac{\mu}{2}\int_{\Delta y}\left(\overline{v}_2 + V_2^r - \overline{v}_2 - V_2^l\right)dy + \frac{\mu}{2}\int_{\Delta x}\left(\overline{v}_1 + V_1^t - \overline{v}_1 - V_1^b\right)dx = \\
&= \frac{\mu}{2}\int_{\Delta y}\left(V_2^r - V_2^l\right)dy + \frac{\mu}{2}\int_{\Delta x}\left(V_1^t - V_1^b\right)dx \approx \\
&\approx \frac{\mu}{3}\Delta y\left(V_2^{rc} - V_2^{lc}\right) + \frac{\mu}{12}\Delta y\left(V_2^{rt} + V_2^{rd} - V_2^{lt} - V_2^{lb}\right) + \\
&+ \frac{\mu}{3}\Delta x\left(V_1^{tc} - V_1^{bc}\right) + \frac{\mu}{12}\Delta x\left(V_1^{tr} + V_1^{tl} - V_1^{br} - V_1^{bl}\right),
\end{aligned}
\tag{19}
$$

for the shear stress, and

$$
\begin{aligned}
&\int_{\Delta x}\int_{\Delta y}\dot{\sigma}_{22}dxdy = \lambda\int_{\Delta y}\left(v_1^r - v_1^l\right)dy + (\lambda+2\mu)\int_{\Delta x}\left(v_2^t - v_2^b\right)dx = \\
&= \lambda\int_{\Delta y}\left(\overline{v}_1 + V_1^r - \overline{v}_1 - V_1^l\right)dy + (\lambda+2\mu)\int_{\Delta x}\left(\overline{v}_2 + V_2^t - \overline{v}_2 - V_2^b\right)dx = \\
&= \lambda\int_{\Delta y}\left(V_1^r - V_1^l\right)dy + (\lambda+2\mu)\int_{\Delta x}\left(V_2^t - V_2^b\right)dx \approx \\
&\approx \frac{2}{3}\lambda\Delta y\left(V_1^{rc} - V_1^{lc}\right) + \lambda\frac{1}{6}\Delta y\left(V_1^{rt} + V_1^{rb} - V_1^{lt} - V_1^{lb}\right) + \\
&+ \frac{2}{3}(\lambda+2\mu)\Delta x\left(V_2^{tc} - V_2^{bc}\right) + (\lambda+2\mu)\frac{1}{6}\Delta x\left(V_2^{tr} + V_2^{tl} - V_2^{br} - V_2^{bl}\right),
\end{aligned}
\tag{20}
$$

for the second normal component of the stress tensor, respectively.

Defining averaged values for velocities and stresses

$$
\overline{v}_i = \frac{1}{\Delta x\Delta y}\int_{\Delta x}\int_{\Delta y} v_i dxdy, \quad \overline{\sigma}_{ij} = \frac{1}{\Delta x\Delta y}\int_{\Delta x}\int_{\Delta y}\sigma_{ij}dxdy, \tag{21}
$$

we are ready to formulate a numerical scheme in terms of averaged and excess quantities.

3.3 Numerical scheme

The numerical scheme follows from the standard approximation of time derivatives

$$\dot{f} \approx \frac{f^{k+1} - f^k}{\Delta t} \quad \forall f, \tag{22}$$

which, accounting for Eqs. (16) and (17), results in

$$\begin{aligned}(\rho\overline{v}_1)^{k+1} - (\rho\overline{v}_1)^k = \frac{2}{3}\frac{\Delta t}{\Delta x}\left(\Sigma_{11}^{rc} - \Sigma_{11}^{lc}\right) + \frac{1}{6}\frac{\Delta t}{\Delta x}\left(\Sigma_{11}^{rt} + \Sigma_{11}^{rb} - \Sigma_{11}^{lt} - \Sigma_{11}^{lb}\right) + \\ + \frac{2}{3}\frac{\Delta t}{\Delta y}\left(\Sigma_{12}^{tc} - \Sigma_{12}^{bc}\right) + \frac{1}{6}\frac{\Delta t}{\Delta y}\left(\Sigma_{12}^{tr} + \Sigma_{12}^{tl} - \Sigma_{12}^{br} - \Sigma_{12}^{bl}\right),\end{aligned} \tag{23}$$

$$\begin{aligned}(\rho\overline{v}_2)^{k+1} - (\rho\overline{v}_2)^k = \frac{2}{3}\frac{\Delta t}{\Delta x}\left(\Sigma_{21}^{rc} - \Sigma_{21}^{lc}\right) + \frac{1}{6}\frac{\Delta t}{\Delta x}\left(\Sigma_{21}^{rt} + \Sigma_{21}^{rb} - \Sigma_{21}^{lt} - \Sigma_{21}^{lb}\right) + \\ + \frac{2}{3}\frac{\Delta t}{\Delta y}\left(\Sigma_{22}^{tc} - \Sigma_{22}^{bc}\right) + \frac{1}{6}\frac{\Delta t}{\Delta y}\left(\Sigma_{22}^{tr} + \Sigma_{22}^{tl} - \Sigma_{22}^{br} - \Sigma_{22}^{bl}\right),\end{aligned} \tag{24}$$

for the averaged velocities for each cell n, m. Here all the quantities in the right hand side are given at time step k and the matter density ρ is assumed to be constant inside each computational cell.

Similarly, for averaged stress components in each cell n, m we have

$$\begin{aligned}(\overline{\sigma}_{11})^{k+1} - (\overline{\sigma}_{11})^k = (\lambda + 2\mu)\frac{2}{3}\frac{\Delta t}{\Delta x}\left(V_1^{rc} - V_1^{lc}\right) + \\ + (\lambda + 2\mu)\frac{1}{6}\frac{\Delta t}{\Delta x}\left(V_1^{rt} + V_1^{rb} - V_1^{lt} - V_1^{lb}\right) + \lambda\frac{2}{3}\frac{\Delta t}{\Delta y}\left(V_2^{tc} - V_2^{bc}\right) + \\ + \lambda\frac{1}{6}\frac{\Delta t}{\Delta y}\left(V_2^{tr} + V_2^{tl} - V_2^{br} - V_2^{bl}\right),\end{aligned} \tag{25}$$

$$\begin{aligned}(\overline{\sigma}_{22})^{k+1} - (\overline{\sigma}_{22})^k = \lambda\frac{2}{3}\frac{\Delta t}{\Delta x}\left(V_1^{rc} - V_1^{lc}\right) + \lambda\frac{1}{6}\frac{\Delta t}{\Delta x}\left(V_1^{rt} + V_1^{rb} - V_1^{lt} - V_1^{lb}\right) + \\ + (\lambda + 2\mu)\frac{2}{3}\frac{\Delta t}{\Delta y}\left(V_2^{tc} - V_2^{bc}\right) + (\lambda + 2\mu)\frac{1}{6}\frac{\Delta t}{\Delta y}\left(V_2^{tr} + V_2^{tl} - V_2^{br} - V_2^{bl}\right),\end{aligned} \tag{26}$$

$$\begin{aligned}(\overline{\sigma}_{12})^{k+1} - (\overline{\sigma}_{12})^k = \frac{1}{3}\mu\frac{\Delta t}{\Delta x}\left(V_2^{rc} - V_2^{lc}\right) + \frac{1}{12}\mu\frac{\Delta t}{\Delta x}\left(V_2^{rt} + V_2^{rb} - V_2^{lt} - V_2^{lb}\right) + \\ + \frac{1}{3}\mu\frac{\Delta t}{\Delta y}\left(V_1^{tc} - V_1^{bc}\right) + \frac{1}{12}\mu\frac{\Delta t}{\Delta y}\left(V_1^{tr} + V_1^{tl} - V_1^{br} - V_1^{bl}\right).\end{aligned} \tag{27}$$

Numerical scheme (23)–(27) is written down in terms of excess quantities. Therefore, the necessary step is to determine values of excess quantities. Numerical scheme (23)–(27) uses the values of excess quantities at the middle points of cell boundaries.

It is reasonable to identify these values with the values of average excess quantities (i.e., $V_1^{rc} = \overline{V}_1^r$, etc).

4 Determination of excess quantities

4.1 Averaged excess quantities

4.1.1 Normal components

Averaged values of excess quantities are determined exactly by means of jump relations at boundaries between computational cells, which express the continuity of true stresses and velocities (Berezovski et al., 2008)

$$\left[\left[\overline{\sigma}_{ij} + \Sigma_{ij}\right]\right] = 0, \quad [\![\overline{v}_i + \mathcal{V}_i]\!] = 0. \tag{28}$$

In terms of normal components these jump relations for each time step result in

$$(\overline{\sigma}_{11})_{n-1\,m} + \left(\overline{\Sigma}_{11}^r\right)_{n-1\,m} = (\overline{\sigma}_{11})_{n\,m} + \left(\overline{\Sigma}_{11}^l\right)_{n\,m}, \tag{29}$$

$$(\overline{\sigma}_{22})_{n\,m-1} + \left(\overline{\Sigma}_{22}^t\right)_{n\,m-1} = (\overline{\sigma}_{22})_{n\,m} + \left(\overline{\Sigma}_{22}^b\right)_{n\,m}, \tag{30}$$

for stresses and

$$(\overline{v}_1)_{n-1\,m} + \left(\overline{V}_1^r\right)_{n-1\,m} = (\overline{v}_1)_{n\,m} + \left(\overline{V}_1^l\right)_{n\,m}, \tag{31}$$

$$(\overline{v}_2)_{n\,m-1} + \left(\overline{V}_2^t\right)_{n\,m-1} = (\overline{v}_2)_{n\,m} + \left(\overline{V}_2^b\right)_{n\,m}, \tag{32}$$

for velocities. In both cases we have only two equations for four averaged excess quantities. The closure of these systems of equations is achieved by means of conditions of the conservation of "Riemann invariants" for excess quantities (Berezovski, 2011)

$$\left(\rho c_p \overline{V}_1^l\right)_{n\,m} + \left(\overline{\Sigma}_{11}^l\right)_{n\,m} = 0, \tag{33}$$

$$\left(\rho c_p \overline{V}_1^r\right)_{n-1\,m} - \left(\overline{\Sigma}_{11}^r\right)_{n-1\,m} = 0, \tag{34}$$

$$\left(\rho c_p \overline{V}_2^b\right)_{n\,m} + \left(\overline{\Sigma}_{22}^b\right)_{n\,m} = 0, \tag{35}$$

$$\left(\rho c_p \overline{V}_2^t\right)_{n\,m-1} - \left(\overline{\Sigma}_{22}^t\right)_{n\,m-1} = 0, \tag{36}$$

which leads to closed systems of equations for averaged excess velocities

$$(\overline{\sigma}_{11})_{n-1\,m} + \left(\rho c_p \overline{V}_1^r\right)_{n-1\,m} = (\overline{\sigma}_{11})_{n\,m} - \left(\rho c_p \overline{V}_1^l\right)_{n\,m}, \tag{37}$$

$$(\overline{v}_1)_{n-1\,m} + \left(\overline{V}_1^r\right)_{n-1\,m} = (\overline{v}_1)_{n\,m} + \left(\overline{V}_1^l\right)_{n\,m}, \tag{38}$$

and

$$(\overline{\sigma}_{22})_{n\,m-1} + \left(\rho c_p \overline{V}_2^t\right)_{n\,m-1} = (\overline{\sigma}_{22})_{n\,m} - \left(\rho c_p \overline{V}_2^b\right)_{n\,m}, \tag{39}$$

$$(\overline{v}_2)_{n\,m-1} + \left(\overline{V}_2^t\right)_{n\,m-1} = (\overline{v}_2)_{n\,m} + \left(\overline{V}_2^b\right)_{n\,m}. \tag{40}$$

Both systems of equations (37)–(38) and (39)–(40) have explicit exact solutions. The solution of the first system of equations reads

$$\left(\overline{V}_1^r\right)_{n-1\,m} = \frac{(\overline{\sigma}_{11})_{n\,m} - (\overline{\sigma}_{11})_{n-1\,m} + \left(\rho c_p\right)_{n\,m}\left[(\overline{v}_1)_{n\,m} - (\overline{v}_1)_{n-1\,m}\right]}{\left[\left(\rho c_p\right)_{n-1\,m} + \left(\rho c_p\right)_{n\,m}\right]}, \tag{41}$$

and

$$\left(\overline{V}_1^l\right)_{n\,m} = \frac{(\overline{\sigma}_{11})_{n\,m} - (\overline{\sigma}_{11})_{n-1\,m} - \left(\rho c_p\right)_{n-1\,m}\left[(\overline{v}_1)_{n\,m} - (\overline{v}_1)_{n-1\,m}\right]}{\left[\left(\rho c_p\right)_{n-1\,m} + \left(\rho c_p\right)_{n\,m}\right]}. \tag{42}$$

Corresponding excess values of normal components of the stress tensor follow from the conservation of Riemann invariants

$$\left(\overline{\Sigma}_{11}^l\right)_{n\,m} = -\left(\rho c_p \overline{V}_1^l\right)_{n\,m}, \tag{43}$$

$$\left(\overline{\Sigma}_{11}^r\right)_{n-1\,m} = \left(\rho c_p \overline{V}_1^r\right)_{n-1\,m}. \tag{44}$$

Accordingly, the solution of the second system of equations (39)–(40) has the form

$$\left(\overline{V}_2^t\right)_{n\,m-1} = \frac{(\overline{\sigma}_{22})_{n\,m} - (\overline{\sigma}_{22})_{n\,m-1} + \left(\rho c_p\right)_{n\,m}\left[(\overline{v}_2)_{n\,m} - (\overline{v}_2)_{n\,m-1}\right]}{\left[\left(\rho c_p\right)_{n\,m-1} + \left(\rho c_p\right)_{n\,m}\right]}, \tag{45}$$

$$\left(\overline{V}_2^b\right)_{n\,m} = \frac{(\overline{\sigma}_{22})_{n\,m} - (\overline{\sigma}_{22})_{n\,m-1} - \left(\rho c_p\right)_{n\,m-1}\left[(\overline{v}_2)_{n\,m} - (\overline{v}_2)_{n\,m-1}\right]}{\left[\left(\rho c_p\right)_{n\,m-1} + \left(\rho c_p\right)_{n\,m}\right]}, \tag{46}$$

with excess values of normal components of the stress tensor

$$\left(\overline{\Sigma}_{22}^b\right)_{n\,m} = -\left(\rho c_p \overline{V}_2^b\right)_{n\,m}, \tag{47}$$

$$\left(\overline{\Sigma}_{22}^t\right)_{n\,m-1} = \left(\rho c_p \overline{V}_2^t\right)_{n\,m-1}. \tag{48}$$

4.1.2 Shear components

The values of excess quantities for shear components of the stress tensor are still determined by means of jump relations at boundaries between computational cells (28). In terms of shear components these jump relations result in

$$(\overline{\sigma}_{21})_{n-1\,m} + \left(\overline{\Sigma}^{r}_{21}\right)_{n-1\,m} = (\overline{\sigma}_{21})_{n\,m} + \left(\overline{\Sigma}^{l}_{21}\right)_{n\,m}, \tag{49}$$

$$(\overline{\sigma}_{12})_{n\,m-1} + \left(\overline{\Sigma}^{t}_{12}\right)_{n\,m-1} = (\overline{\sigma}_{12})_{n\,m} + \left(\overline{\Sigma}^{b}_{12}\right)_{n\,m}, \tag{50}$$

for stresses and

$$(\overline{v}_{1})_{n\,m-1} + \left(\overline{V}^{t}_{1}\right)_{n\,m-1} = (\overline{v}_{1})_{n\,m} + \left(\overline{V}^{b}_{1}\right)_{n\,m}, \tag{51}$$

$$(\overline{v}_{2})_{n-1\,m} + \left(\overline{V}^{r}_{2}\right)_{n-1\,m} = (\overline{v}_{2})_{n\,m} + \left(\overline{V}^{l}_{2}\right)_{n\,m}, \tag{52}$$

for corresponding velocities. The closure of systems of equations is again achieved by means of conditions of the conservation of "Riemann invariants" for corresponding excess quantities

$$\left(\overline{\Sigma}^{b}_{12}\right)_{n\,m} = -\left(\rho c_s \overline{V}^{b}_{1}\right)_{n\,m}, \tag{53}$$

$$\left(\overline{\Sigma}^{t}_{12}\right)_{n\,m-1} = \left(\rho c_s \overline{V}^{t}_{1}\right)_{n\,m-1}, \tag{54}$$

$$\left(\overline{\Sigma}^{l}_{21}\right)_{n\,m} = -\left(\rho c_s \overline{V}^{l}_{2}\right)_{n\,m}, \tag{55}$$

$$\left(\overline{\Sigma}^{r}_{21}\right)_{n-1\,m} = \left(\rho c_s \overline{V}^{r}_{2}\right)_{n-1\,m}. \tag{56}$$

Explicit exact solutions for excess quantities of shear components are still exist in the form

$$\left(\overline{V}^{r}_{2}\right)_{n-1\,m} = \frac{(\overline{\sigma}_{21})_{n\,m} - (\overline{\sigma}_{21})_{n-1\,m} + (\rho c_s)_{n\,m}\left[(\overline{v}_{2})_{n\,m} - (\overline{v}_{2})_{n-1\,m}\right]}{\left[(\rho c_s)_{n-1\,m} + (\rho c_s)_{n\,m}\right]}, \tag{57}$$

$$\left(\overline{V}^{l}_{2}\right)_{n\,m} = \frac{(\overline{\sigma}_{21})_{n\,m} - (\overline{\sigma}_{21})_{n-1\,m} - (\rho c_s)_{n-1\,m}\left[(\overline{v}_{2})_{n\,m} - (\overline{v}_{2})_{n-1\,m}\right]}{\left[(\rho c_s)_{n-1\,m} + (\rho c_s)_{n\,m}\right]}, \tag{58}$$

and

$$\left(\overline{V}^{t}_{1}\right)_{n\,m-1} = \frac{(\overline{\sigma}_{12})_{n\,m} - (\overline{\sigma}_{12})_{n\,m-1} + (\rho c_s)_{n\,m}\left[(\overline{v}_{1})_{n\,m} - (\overline{v}_{1})_{n\,m-1}\right]}{\left[(\rho c_s)_{n\,m-1} + (\rho c_s)_{n\,m}\right]}, \tag{59}$$

$$\left(\overline{V}^{b}_{1}\right)_{n\,m} = \frac{(\overline{\sigma}_{12})_{n\,m} - (\overline{\sigma}_{12})_{n\,m-1} - (\rho c_s)_{n\,m-1}\left[(\overline{v}_{1})_{n\,m} - (\overline{v}_{1})_{n\,m-1}\right]}{\left[(\rho c_s)_{n\,m-1} + (\rho c_s)_{n\,m}\right]}. \tag{60}$$

Values of averaged excess quantities for shear components of the stress tensor follow from the conservation of Riemann invariants mentioned above. Now all averaged excess quantities are determined. It remains to calculate the values of excess quantities at the corners of computational cells.

4.2 Excess quantities at vertices

Suppose that values of velocity $(V_1^{tr})_{n\,m}$ at upper right corner of the cell numbered (n, m) is known.

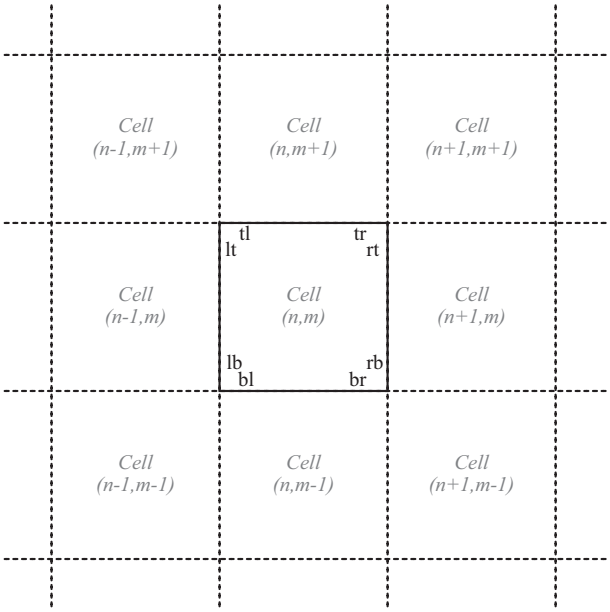

Fig. 2 Notation for neighbouring cells

It should be noted that each corner of the computational cell $C_{n\,m} = [x_n, x_{n+1}] \times [y_m, y_{m+1}]$ can be considered as the central point of one of the corresponding four virtual cells $C_{n\pm1/2\,m\pm1/2} = [x_{n\pm1/2}, x_{n+1\pm1/2}] \times [y_{m\pm1/2}, y_{m+1\pm1/2}]$. In the first approximation, the value of every field quantity at corners of computational cells can be represented as the simple average of the corresponding values in neighbouring cells (see the notation in Fig. 2). This means that the value of the horizontal excess velocity at the right upper corner $(V_1^{rt})_{n\,m}$ is calculated by the expression

$$\begin{aligned}(\overline{v}_1)_{n\,m} + (V_1^{rt})_{n\,m} = \frac{1}{4}\Big((\overline{v}_1)_{n\,m} + \left(\overline{V}_1^{r}\right)_{n\,m} + (\overline{v}_1)_{n,\,m+1} + \left(\overline{V}_1^{r}\right)_{n\,m+1} + \\ + (\overline{v}_1)_{n+1\,m} + \left(\overline{V}_1^{l}\right)_{n+1\,m} + (\overline{v}_1)_{n+1,\,m+1} + \left(\overline{V}_1^{l}\right)_{n+1\,m+1}\Big),\end{aligned} \tag{61}$$

which results in

$$\begin{aligned}(V_1^{rt})_{n\,m} = \frac{1}{4}\Big(-3\,(\overline{v}_1)_{n\,m} + \left(\overline{V}_1^{r}\right)_{n\,m} + (\overline{v}_1)_{n,\,m+1} + \left(\overline{V}_1^{r}\right)_{n\,m+1} + \\ + (\overline{v}_1)_{n+1\,m} + \left(\overline{V}_1^{l}\right)_{n+1\,m} + (\overline{v}_1)_{n+1,\,m+1} + \left(\overline{V}_1^{l}\right)_{n+1\,m+1}\Big).\end{aligned} \tag{62}$$

It is clear that due to symmetry of averaging the value of another velocity component $(V_1^{tr})_{n\,m}$ is the same

$$(V_1^{tr})_{n\,m} = (V_1^{rt})_{n\,m}. \tag{63}$$

Similarly, for $(V_1^{rb})_{n\,m}$ we have

$$\begin{aligned}(V_1^{rb})_{n\,m} =& \frac{1}{4}\left(-3\,(\overline{v}_1)_{n\,m} + \left(\overline{V}_1^{r}\right)_{n\,m} + (\overline{v}_1)_{n,\,m-1} + \left(\overline{V}_1^{r}\right)_{n\,m-1} + \right.\\ &\left. + (\overline{v}_1)_{n+1\,m} + \left(\overline{V}_1^{l}\right)_{n+1\,m} + (\overline{v}_1)_{n+1,\,m-1} + \left(\overline{V}_1^{l}\right)_{n+1\,m-1}\right),\end{aligned} \tag{64}$$

with

$$(V_1^{br})_{n\,m} = (V_1^{rb})_{n\,m}. \tag{65}$$

Remaining values of excess velocities at corners of computational cells are determined in the same way. Namely,

$$\begin{aligned}(V_1^{lt})_{n\,m} =& \frac{1}{4}\left(-3\,(\overline{v}_1)_{n\,m} + \left(\overline{V}_1^{l}\right)_{n\,m} + (\overline{v}_1)_{n,\,m+1} + \left(\overline{V}_1^{l}\right)_{n\,m+1} + \right.\\ &\left. + (\overline{v}_1)_{n-1\,m} + \left(\overline{V}_1^{r}\right)_{n-1\,m} + (\overline{v}_1)_{n-1,\,m+1} + \left(\overline{V}_1^{r}\right)_{n-1\,m+1}\right),\end{aligned} \tag{66}$$

$$\begin{aligned}(V_1^{lb})_{n\,m} =& \frac{1}{4}\left(-3\,(\overline{v}_1)_{n\,m} + \left(\overline{V}_1^{l}\right)_{n\,m} + (\overline{v}_1)_{n,\,m-1} + \left(\overline{V}_1^{l}\right)_{n\,m-1} + \right.\\ &\left. (\overline{v}_1)_{n-1\,m} + \left(\overline{V}_1^{r}\right)_{n-1\,m} + (\overline{v}_1)_{n-1,\,m-1} + \left(\overline{V}_1^{r}\right)_{n-1\,m-1}\right).\end{aligned} \tag{67}$$

The same rules of averaging are used for excess stress components. For instance, we have for $(\Sigma_{11}^{rt})_{n\,m}$

$$\begin{aligned}(\Sigma_{11}^{rt})_{n\,m} =& \frac{1}{4}\left(-3\,(\overline{\sigma}_{11})_{n\,m} + \left(\overline{\Sigma}_{11}^{r}\right)_{n\,m} + (\overline{\sigma}_{11})_{n,\,m+1} + \left(\overline{\Sigma}_{11}^{r}\right)_{n\,m+1} + \right.\\ &\left. + (\overline{\sigma}_{11})_{n+1\,m} + \left(\overline{\Sigma}_{11}^{l}\right)_{n+1\,m} + (\overline{\sigma}_{11})_{n+1,\,m+1} + \left(\overline{\Sigma}_{11}^{l}\right)_{n+1\,m+1}\right),\end{aligned} \tag{68}$$

and, consecutively,

$$\begin{aligned}(\Sigma_{11}^{rb})_{n\,m} =& \frac{1}{4}\left(-3\,(\overline{\sigma}_{11})_{n\,m} + \left(\overline{\Sigma}_{11}^{r}\right)_{n\,m} + (\overline{\sigma}_{11})_{n,\,m-1} + \left(\overline{\Sigma}_{11}^{r}\right)_{n\,m-1} + \right.\\ &\left. + (\overline{\sigma}_{11})_{n+1\,m} + \left(\overline{\Sigma}_{11}^{l}\right)_{n+1\,m} + (\overline{\sigma}_{11})_{n+1,\,m-1} + \left(\overline{\Sigma}_{11}^{l}\right)_{n+1\,m-1}\right),\end{aligned} \tag{69}$$

$$(\Sigma_{11}^{lt})_{n\,m} = \frac{1}{4}\left(-3\,(\overline{\sigma}_{11})_{n\,m} + \left(\overline{\Sigma}_{11}^{l}\right)_{n\,m} + (\overline{\sigma}_{11})_{n,\,m+1} + \left(\overline{\Sigma}_{11}^{l}\right)_{n\,m+1} + \right.$$
$$\left. + (\overline{\sigma}_{11})_{n-1\,m} + \left(\overline{\Sigma}_{11}^{r}\right)_{n-1\,m} + (\overline{\sigma}_{11})_{n-1,\,m+1} + \left(\overline{\Sigma}_{11}^{r}\right)_{n-1\,m+1}\right), \tag{70}$$

$$(\Sigma_{11}^{lb})_{n\,m} = \frac{1}{4}\left(-3\,(\overline{\sigma}_{11})_{n\,m} + \left(\overline{\Sigma}_{11}^{l}\right)_{n\,m} + (\overline{\sigma}_{11})_{n,\,m-1} + \left(\overline{\Sigma}_{11}^{l}\right)_{n\,m-1} + \right.$$
$$\left. (\overline{\sigma}_{11})_{n-1\,m} + \left(\overline{\Sigma}_{11}^{r}\right)_{n-1\,m} + (\overline{\sigma}_{11})_{n-1,\,m-1} + \left(\overline{\Sigma}_{11}^{r}\right)_{n-1\,m-1}\right), \tag{71}$$

All other excess quantities at corners of computational cells are calculated algebraically in the same way. This finalizes the procedure of the determination of excess quantities. The substitution of the values of excess quantities into numerical scheme (23)–(27) allows us to perform calculations of two-dimensional problems.

5 Test problem

As an example, a stress pulse propagation in a waveguide depicted in Fig. 3 is considered. The length of the waveguide is 250 mm, its thickness is 100 mm.

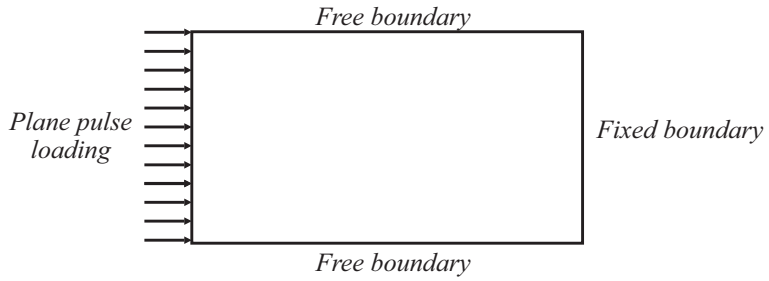

Fig. 3 Boundary conditions

Calculations are performed for Al 6061 alloy characterized by the density 2700 kg/m^3, the Young modulus 68.9 GPa, and the Poisson ratio 0.33. This corresponds to the longitudinal wave velocity 5092 m/s. Choosing the space step equal to 1 mm, we have the time step 0.196 μs.

To be able to perform the calculation of a particular problem we need to specify initial and boundary conditions. Initial conditions fix the state of each cell at a chosen time instant. We suppose that initially the waveguide is at rest, which assumes zero values for all wanted fields. Boundary conditions should be expressed in terms of averaged and excess quantities used in the numerical scheme. We expect that the state of cells adjacent to each boundary is known (at least partly). For the proper computing, we need to know in advance as many values of averaged and excess quantities as possible.

5.1 Upper boundary: stress-free

We start with the stress-free upper boundary conditions. It should be noted that the implementation of stress-free boundary conditions in the numerical scheme is not easy task. The main progress in this direction is achieved by the geophysical community (Moczo et al., 2014). There the free-surface boundary treatment is performed within the finite-difference framework because of the efficiency of wave motion simulation in comparison with finite element or discontinuous Galerkin methods (Gao et al., 2015).

However, in the proposed numerical procedure all the boundary conditions need to be formulated in terms of averaged and excess quantities. As we know, jump relations at boundaries between computational cells express continuity of true stresses and velocities (28) It follows that at the stress-free upper boundary the value of the normal stress is zero yielding (for each time step)

$$(\overline{\sigma}_{22})_n + \left(\overline{\Sigma}^t_{22}\right)_n = 0. \tag{72}$$

A similar relationship holds for the shear stress

$$(\overline{\sigma}_{12})_n + \left(\overline{\Sigma}^t_{12}\right)_n = 0. \tag{73}$$

Additionally, since values of the normal and shear stresses at the stress-free boundary are not evolving with time, we have for $\Delta x = \Delta y$

$$\begin{aligned}
&\lambda\left(\left(\overline{V}^r_1\right)_n - \left(\overline{V}^l_1\right)_n\right) + (\lambda+2\mu)\left(\left(\overline{V}^t_2\right)_n - \left(\overline{V}^b_2\right)_n\right) + \\
&+\frac{\lambda}{4}\left(\left(\overline{V}^{rt}_1\right)_n + \left(\overline{V}^{rb}_1\right)_n - \left(\overline{V}^{lt}_1\right)_n - \left(\overline{V}^{lb}_1\right)_n\right) + \\
&+\frac{(\lambda+2\mu)}{4}\left(\left(\overline{V}^{tr}_2\right)_n + \left(\overline{V}^{tl}_2\right)_n - \left(\overline{V}^{br}_2\right)_n - \left(\overline{V}^{bl}_2\right)_n\right) = 0,
\end{aligned} \tag{74}$$

$$\begin{aligned}
&\left(\left(\overline{V}^r_2\right)_n - \left(\overline{V}^l_2\right)_n\right) + + \left(\left(\overline{V}^t_1\right)_n - \left(\overline{V}^b_1\right)_n\right) + \\
&+\frac{1}{4}\left(\left(\overline{V}^{rt}_2\right)_n + \left(\overline{V}^{rb}_2\right)_n - \left(\overline{V}^{lt}_2\right)_n - \left(\overline{V}^{lb}_2\right)_n\right) + \\
&\frac{1}{4}\left(\left(\overline{V}^{tr}_1\right)_n + \left(\overline{V}^{tl}_1\right)_n - \left(\overline{V}^{br}_1\right)_n - \left(\overline{V}^{bl}_1\right)_n\right) = 0.
\end{aligned} \tag{75}$$

Equations (72) – (75) allow us to calculate values of four excess quantities, namely, $\left(\overline{V}^t_1\right)_n$, $\left(\overline{V}^t_2\right)_n$, $\left(\overline{\Sigma}^t_{12}\right)_n$, and $\left(\overline{\Sigma}^t_{22}\right)_n$, at the upper stress-free boundary. Fortunately, it is sufficient to update the averaged values of all fields at the upper layer of the computational domain.

The similar consideration is valid for the stress-free bottom boundary with the corresponding transformation of indices.

5.2 Left boundary: loading

At the loading left boundary the value of the normal stress in each cell and at each time step is given in advance

$$(\overline{\sigma}_{11})_m + \left(\overline{\Sigma}^l_{11}\right)_m = \sigma_{11}(t), \tag{76}$$

where $\sigma_{11}(t)$ is a known function. A similar relationship holds for the shear stress

$$(\overline{\sigma}_{12})_m + \left(\overline{\Sigma}^l_{12}\right)_m = \sigma_{12}(t). \tag{77}$$

Since values of the normal and shear stresses at the loading boundary are evolving with time, we have additionally for each boundary cell and at each time step

$$\begin{aligned}\Delta x\dot{\sigma}_{11} = {} & \frac{2}{3}(\lambda+2\mu)\left[\left(\overline{V}^r_1\right)_m - \left(\overline{V}^l_1\right)_m\right] + \frac{2}{3}\lambda\left[\left(\overline{V}^t_2\right)_m - \left(\overline{V}^b_2\right)_m\right] + \\ & + (\lambda+2\mu)\frac{1}{6}\left(\left(\overline{V}^{rt}_1\right)_m + \left(\overline{V}^{rb}_1\right)_m - \left(\overline{V}^{lt}_1\right)_m - \left(\overline{V}^{lb}_1\right)_m\right) + \\ & + \lambda\frac{1}{6}\left(\left(\overline{V}^{tr}_2\right)_m + \left(\overline{V}^{tl}_2\right)_m - \left(\overline{V}^{br}_2\right)_m - \left(\overline{V}^{bl}_2\right)_m\right),\end{aligned} \tag{78}$$

$$\begin{aligned}\Delta x\dot{\sigma}_{12} = {} & \frac{1}{3}\mu\left[\left(\overline{V}^r_2\right)_m - \left(\overline{V}^l_2\right)_m\right] + \frac{1}{3}\mu\left[\left(\overline{V}^t_1\right)_m - \left(\overline{V}^b_1\right)_m\right] + \\ & + \frac{1}{12}\mu\left(\left(\overline{V}^{rt}_2\right)_m + \left(\overline{V}^{rb}_2\right)_m - \left(\overline{V}^{lt}_2\right)_m - \left(\overline{V}^{lb}_2\right)_m\right) + \\ & + \frac{1}{12}\mu\left(\left(\overline{V}^{tr}_1\right)_m + \left(\overline{V}^{tl}_1\right)_m - \left(\overline{V}^{br}_1\right)_m - \left(\overline{V}^{bl}_1\right)_m\right).\end{aligned} \tag{79}$$

By means of equations (76) – (79) we can calculate values of four excess quantities, namely, $\left(\overline{V}^l_1\right)_m$, $\left(\overline{V}^l_2\right)_m$, $\left(\overline{\Sigma}^l_1\right)_m$, and $\left(\overline{\Sigma}^l_2\right)_m$, at the left boundary. As previously, it is sufficient to update the averaged values of all fields at the left boundary of the computational domain.

5.3 Right boundary: fixed

At a fixed right boundary the values of velocities are zero, i.e.,

$$(\overline{v}_i)_m + \left(\overline{V}^r_i\right)_m = 0, \quad \forall\, m. \tag{80}$$

Besides, since values of velocities at the fixed boundary are not evolving with time, we have $\forall\, m$

$$\left(\left(\overline{\Sigma}^{r}_{11}\right)_m - \left(\overline{\Sigma}^{l}_{11}\right)_m\right) + \left(\left(\overline{\Sigma}^{t}_{12}\right)_m - \left(\overline{\Sigma}^{b}_{12}\right)_m\right) + \\ + \frac{1}{4}\left(\left(\overline{\Sigma}^{rt}_{11}\right)_m + \left(\overline{\Sigma}^{rb}_{11}\right)_m - \left(\overline{\Sigma}^{lt}_{11}\right)_m - \left(\overline{\Sigma}^{lb}_{11}\right)_m\right) + \\ + \frac{1}{4}\left(\left(\overline{\Sigma}^{tr}_{12}\right)_m + \left(\overline{\Sigma}^{tl}_{12}\right)_m - \left(\overline{\Sigma}^{br}_{12}\right)_m - \left(\overline{\Sigma}^{bl}_{12}\right)_m\right) = 0, \tag{81}$$

$$\left(\left(\overline{\Sigma}^{r}_{21}\right)_m - \left(\overline{\Sigma}^{l}_{21}\right)_m\right) + \left(\left(\overline{\Sigma}^{t}_{22}\right)_m - \left(\overline{\Sigma}^{b}_{22}\right)_m\right) + \\ + \frac{1}{4}\left(\left(\overline{\Sigma}^{rt}_{21}\right)_m + \left(\overline{\Sigma}^{rb}_{21}\right)_m - \left(\overline{\Sigma}^{lt}_{21}\right)_m - \left(\overline{\Sigma}^{lb}_{21}\right)_m\right) + \\ + \frac{1}{4}\left(\left(\overline{\Sigma}^{tr}_{22}\right)_m + \left(\overline{\Sigma}^{tl}_{22}\right)_m - \left(\overline{\Sigma}^{br}_{22}\right)_m - \left(\overline{\Sigma}^{bl}_{22}\right)_m\right) = 0. \tag{82}$$

Relatioships (80) – (82) are served to obtain values of four excess quantities, namely, $\left(\overline{V}^{r}_{1}\right)_m$, $\left(\overline{V}^{r}_{2}\right)_m$, $\left(\overline{\Sigma}^{r}_{11}\right)_m$, and $\left(\overline{\Sigma}^{r}_{21}\right)_m$, at the fixed right boundary. As before, it is sufficient to update the averaged values of all fields at the right layer of the computational domain.

5.4 Results of computations

The problem of a pulse propagation in an homogeneous waveguide is solved by means of wave-propagation algorithm (LeVeque, 1997) and by means of the proposed numerical scheme. The shape of the plane loading pulse at the left boundary is prescribed by the dependence $\sigma_{11}(t) = \sin^2(\pi t/80)$ for the first 80 time steps. After that the left boundary is stress-free. Calculations were performed for the Courant number 0.91.

The main attention is focused on the influence of lateral boundaries. The distribution of longitudinal stress at 220 time steps presented in the Fig. 4 shows a similarity of results obtained by using the two numerical methods. Here only small difference is observed on the rear side of the pulse.

However, the distinction in the distribution of the longitudinal stress becomes more evident after reflection at the fixed right boundary as one can see in Fig. 5. The main difference in these two approaches is in the implementation of boundary conditions. In the wave-propagation algorithm (LeVeque, 2002), boundary conditions are satisfied using the additional "ghost cells". In the proposed thermodynamically consistent scheme, boundary conditions are imposed in terms of excess quantities at boundaries.

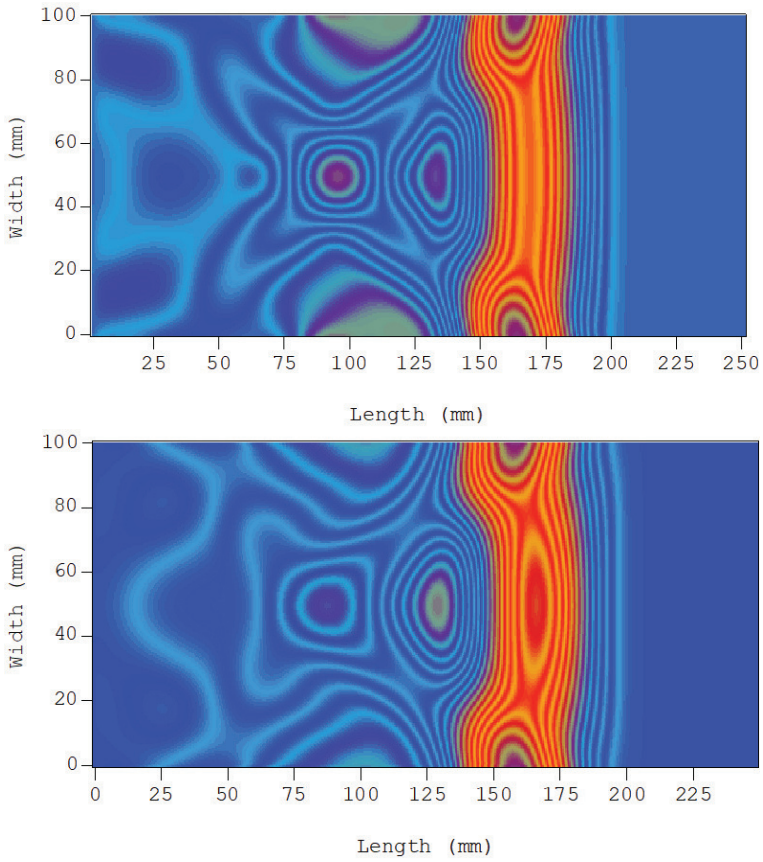

Fig. 4 Contour plot for the longitudinal stress distribution at 220 time steps. Upper panel corresponds to results of the standard wave-propagation algorithm (LeVeque, 2002), bottom panel shows outcome of the proposed numerical scheme.

6 Conclusions

The propagation of a pulse in elastic waveguides displays the result of interactions of distinct modes. Theoretically, only certain first modes are taken into account. Direct numerical simulation combines all of them by default. However, the implementation of boundary conditions should be as accurate as possible. In the paper, such an implementation is proposed in terms of excess quantities taken directly at boundaries. Simulations were performed by means of wave-propagation algorithm (LeVeque, 1997) and by means of the proposed numerical scheme. It should be noted that in the case of plane wave results of calculations obtained by both methods are identical. For non-plane wave, the distribution of longitudinal stress shows a similarity of results obtained by the two numerical methods. However, this similarity is not complete especially after reflection. The details of fields distribution depend

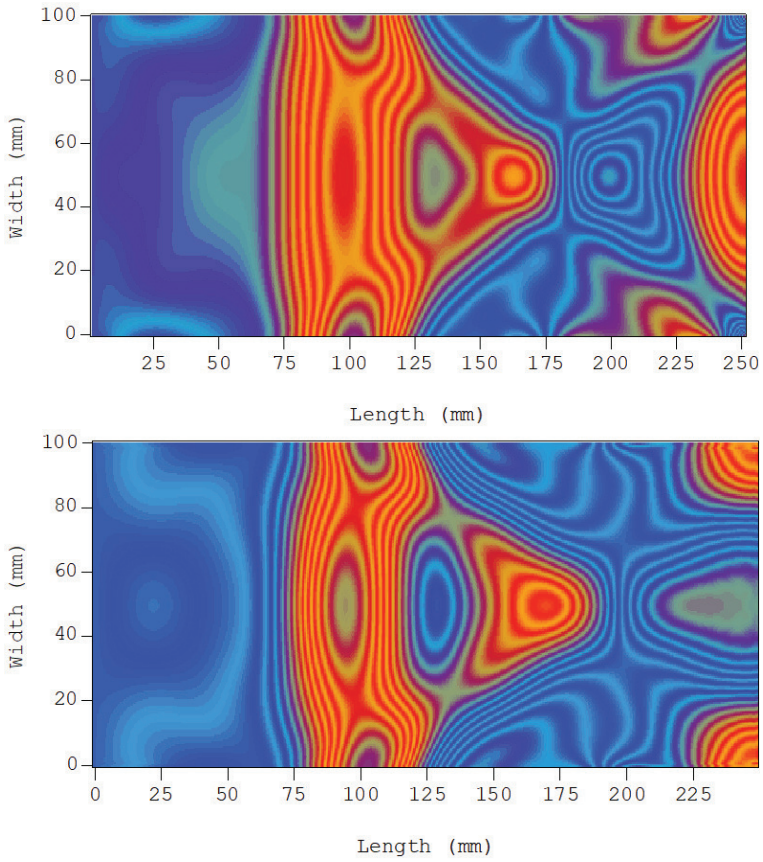

Fig. 5 Contour plot for the longitudinal stress distribution at 480 time steps. Upper panel corresponds to results of the standard wave-propagation algorithm (LeVeque, 2002), bottom panel shows outcome of the proposed numerical scheme.

on the implementation of boundary conditions in the pulse propagation in elastic waveguides.

Acknowledgements
The work is supported by the Centre of Excellence for Nonlinear Dynamic Behaviour of Advanced Materials in Engineering CZ.02.1.01/0.0/0.0/15 003/0000493 (Excellent Research Teams) in the framework of Operational Programme Research, Development and Education, by the Grant project with Nos. 19-04956S of the Czech Science Foundation (CSF) within institutional support RVO:61388998, and by Estonian Research Council under Institutional Research Funding IUT33-24.

References

Abeyaratne R, Knowles JK (2006) Evolution of Phase Transitions: A Continuum Theory. Cambridge University Press

Achenbach J (1973) Wave Propagation in Elastic Solids. Elsevier

Bale DS, LeVeque RJ, Mitran S, Rossmanith JA (2003) A wave propagation method for conservation laws and balance laws with spatially varying flux functions. SIAM Journal on Scientific Computing 24(3):955–978

Berezovski A (2011) Thermodynamic interpretation of finite volume algorithms. Journal of Structural Mechanics (Rakenteiden Mekaniikka) 44(3):156–171

Berezovski A, Maugin G (2001) Simulation of thermoelastic wave propagation by means of a composite wave-propagation algorithm. Journal of Computational Physics 168(1):249–264

Berezovski A, Maugin GA (2002) Thermoelastic wave and front propagation. Journal of Thermal Stresses 25(8):719–743

Berezovski A, Maugin GA (2004) On the thermodynamic conditions at moving phase-transition fronts in thermoelastic solids. Journal of Non-Equilibrium Thermodynamics 29(1):37–51

Berezovski A, Maugin GA (2005a) On the velocity of a moving phase boundary in solids. Acta Mechanica 179(3-4):187–196

Berezovski A, Maugin GA (2005b) Stress-induced phase-transition front propagation in thermoelastic solids. European Journal of Mechanics-A/Solids 24(1):1–21

Berezovski A, Maugin GA (2007) Moving singularities in thermoelastic solids. International Journal of Fracture 147(1-4):191–198

Berezovski A, Maugin GA (2010) Jump conditions and kinetic relations at moving discontinuities. ZAMM-Journal of Applied Mathematics and Mechanics/Zeitschrift für Angewandte Mathematik und Mechanik 90(7-8):537–543

Berezovski A, Engelbrecht J, Maugin G (2000) Thermoelastic wave propagation in inhomogeneous media. Archive of Applied Mechanics 70(10):694–706

Berezovski A, Engelbrecht J, Maugin GA (2003) Numerical simulation of two-dimensional wave propagation in functionally graded materials. European Journal of Mechanics-A/Solids 22(2):257–265

Berezovski A, Berezovski M, Engelbrecht J (2006) Numerical simulation of nonlinear elastic wave propagation in piecewise homogeneous media. Materials Science and Engineering: A 418(1):364–369

Berezovski A, Engelbrecht J, Maugin GA (2008) Numerical Simulation of Waves and Fronts in Inhomogeneous Solids. World Scientific Singapore

Billett S, Toro E (1997) On WAF-type schemes for multidimensional hyperbolic conservation laws. Journal of Computational Physics 130(1):1–24

de Borst R (2008) Challenges in computational materials science: Multiple scales, multi-physics and evolving discontinuities. Computational Materials Science 43(1):1–15

Cohen G (2002) Higher-Order Numerical Methods for Transient Wave Equations. Springer Science & Business Media

Cohen G, Pernet S (2017) Finite Element and Discontinuous Galerkin Methods for Transient Wave Equations. Springer

Colella P (1990) Multidimensional upwind methods for hyperbolic conservation laws. Journal of Computational Physics 87(1):171–200

Dafermos CM (2010) Hyperbolic Conservation Laws in Continuum Physics. Springer, Berlin,

Dumbser M, Käser M (2007) Arbitrary high order non-oscillatory finite volume schemes on unstructured meshes for linear hyperbolic systems. Journal of Computational Physics 221(2):693–723

Gao L, Brossier R, Pajot B, Tago J, Virieux J (2015) An immersed free-surface boundary treatment for seismic wave simulation. Geophysics 80(5):T193–T209

Godlewski E, Raviart PA (1996) Numerical Approximation of Hyperbolic Systems of Conservation Laws. Springer Science & Business Media

Gopalakrishnan S, Chakraborty A, Mahapatra DR (2007) Spectral Finite Element Method: Wave Propagation, Diagnostics and Control in Anisotropic and Inhomogeneous Structures. Springer Science & Business Media

Guinot V (2003) Godunov-type Schemes: An Introduction for Engineers. Elsevier

Hesthaven JS (2018) Numerical Methods for Conservation Laws: From Analysis to Algorithms. SIAM

Hesthaven JS, Warburton T (2007) Nodal Discontinuous Galerkin Methods: Algorithms, Analysis, and Applications. Springer Science & Business Media

Hesthaven JS, Gottlieb S, Gottlieb D (2007) Spectral Methods for Time-dependent Problems. Cambridge University Press

Kampanis NA, Dougalis V, Ekaterinaris JA (2008) Effective Computational Methods for Wave Propagation. Chapman and Hall/CRC

LeVeque RJ (1997) Wave propagation algorithms for multidimensional hyperbolic systems. Journal of Computational Physics 131(2):327–353

LeVeque RJ (2002) Finite Volume Methods for Hyperbolic Problems. Cambridge University Press

Lhomme J, Guinot V (2007) A general approximate-state Riemann solver for hyperbolic systems of conservation laws with source terms. International Journal for Numerical Methods in Fluids 53(9):1509–1540

Liu Y, Shu CW, Tadmor E, Zhang M (2007) Non-oscillatory hierarchical reconstruction for central and finite volume schemes. Communications in Computational Physics 2(5):933–963

Mase GT, Smelser RE, Mase GE (2009) Continuum Mechanics for Engineers. CRC Press

Maugin GA, Berezovski A (2009) On the propagation of singular surfaces in thermoelasticity. Journal of Thermal Stresses 32(6-7):557–592

Moczo P, Kristek J, Gális M (2014) The Finite-Difference Modelling of Earthquake Motions: Waves and Ruptures. Cambridge University Press

Muschik W, Berezovski A (2004) Thermodynamic interaction between two discrete systems in non-equilibrium. Journal of Non-Equilibrium Thermodynamics 29(3):237–255

Roe PL (1981) Approximate Riemann solvers, parameter vectors, and difference schemes. Journal of Computational Physics 43(2):357–372

Roe PL (1986) Discrete models for the numerical analysis of time-dependent multi-dimensional gas dynamics. Journal of Computational Physics 63(2):458–476

Titarev VA, Toro EF (2002) ADER: Arbitrary high order Godunov approach. Journal of Scientific Computing 17(1-4):609–618

Toro EF (1997) Riemann Solvers and Numerical Methods for Fluid Dynamics: A Practical Introduction. Springer Science & Business Media

Trangenstein JA (2009) Numerical Solution of Hyperbolic Partial Differential Equations. Cambridge University Press